CHIN. PHYS. LETT. Vol. 37, No. 11 (2020) 117303

State-Dependent Topological Invariants and Anomalous Bulk-Boundary Correspondence in Non-Hermitian Topological Systems with Generalized Inversion Symmetry

Xiao-Ran Wang(王晓然), Cui-Xian Guo(郭翠仙), Qian Du(杜倩), and Su-Peng Kou(寇谡鹏)*

Center for Advanced Quantum Studies, Department of Physics, Beijing Normal University, Beijing 100875, China

(Received 18 August 2020; accepted 4 October 2020; published online 8 November 2020)

Breakdown of bulk-boundary correspondence in non-Hermitian (NH) topological systems with generalized inversion symmetries is a controversial issue. The non-Bloch topological invariants determine the existence of edge states, but fail to describe the number and distribution of defective edge states in non-Hermitian topological systems. The state-dependent topological invariants, instead of a global topological invariant, are developed to accurately characterize the bulk-boundary correspondence of the NH systems, which is very different from their Hermitian counterparts. At the same time, we obtain the accurate phase diagram of the one-dimensional non-Hermitian Su–Schrieffer–Heeger model with a generalized inversion symmetry from the state-dependent topological invariants. Therefore, these results will be helpful for understanding the exotic topological properties of various non-Hermitian systems.

PACS: 73.90.+f, 73.43.Nq, 73.20.At DOI: 10.1088/0256-307X/37/11/117303

Topological systems, including topological insulators, topological semimetals and topological superconductors, have become the forefront of research in condensed matter physics.[1–9] A signature feature of these topological phases is the topological gapless boundary states immunizing to perturbations, which have been highly regarded because of their exotic properties and potential application in electronic devices. Bulk-boundary correspondence (BBC) is a central principle of topological states. To know whether there exist gapless edge (boundary) states, researchers have just calculated a (global) topological invariant. In general, for the case of finite topological invariant, there exist gapless edge states; for the case of zero topological invariant, there are no gapless edge states.

Recently, topological phases in non-Hermitian (NH) systems have been extensively investigated.[10–73] The combination of topology and non-Hermiticity produces lots of interesting phenomena that have no counterparts in Hermitian, such as the non-Hermitian skin effect,[23,28,33] the breakdown of the bulk-boundary correspondence[17–22,32] and the emergence of the *defective edge state* [an edge state on the ends of an one-dimensional (1D) topological system with NH coalescence].[15,26,57]

However, we find that the non-Bloch invariant can only predict existence of edge states, but cannot exactly characterize their defectiveness. Hence, to completely solve this issue, we develop a new theory for a non-Hermitian topological system with a generalized inversion symmetry by introducing the state-dependent topological invariants. We point out that it is *the state-dependent topological invariants*, rather than *a global state-independent topological invariant*, that characterize the anomalous BBC for non-Hermitian topological phases. With the help of state-dependent topological invariants and effective edge Hamiltonian, we show state-dependent phase diagrams and state-dependent topological transitions for edge states.

One-Dimensional Nonreciprocal Su–Schrieffer–Heeger Model. We take a 1D nonreciprocal Su–Schrieffer–Heeger (SSH) model as an example to explore the underlying physics of anomalous BBC and DESs. The Hamiltonian for the nonreciprocal SSH model with N pairs of lattice sites is given by

$$\begin{aligned}\hat{H} =& (t_1-\gamma)\sum_{n=1}^{N} c_{n,\mathrm{B}}^{\dagger}c_{n,\mathrm{A}} + (t_1+\gamma)\sum_{n=1}^{N} c_{n,\mathrm{A}}^{\dagger}c_{n,\mathrm{B}} \\ &+ t_2\sum_{n=1}^{N-1} c_{n+1,\mathrm{A}}^{\dagger}c_{n,\mathrm{B}} + t_2\sum_{n=1}^{N-1} c_{n,\mathrm{B}}^{\dagger}c_{n+1,\mathrm{A}} \\ &+ \varepsilon\sum_{n=1}^{N} c_{n,\mathrm{A}}^{\dagger}c_{n,\mathrm{A}} - \varepsilon\sum_{n=1}^{N} c_{n,\mathrm{B}}^{\dagger}c_{n,\mathrm{B}}, \end{aligned} \tag{1}$$

where $c_{n,\mathrm{A}}^{\dagger}$ and $c_{n,\mathrm{B}}^{\dagger}$ are the creation operators for electrons on nth unit cell of A and those of B sublattices, respectively; t_1 and t_2 represent the intra-cell and inter-cell hopping strengths, respectively; γ represents the unequal intra-cell hoppings; ε denotes the

Supported by the National Natural Science Foundation of China (Grant Nos. 11674026 and 11974053).
*Corresponding author. Email: spkou@bnu.edu.cn
© 2020 Chinese Physical Society and IOP Publishing Ltd

staggered potential on the two sublattices, which is considered to be a perturbation, and we take $\varepsilon \ll t_2$. Here t_1, t_2, γ, and ε are all real. In this study, we set $t_2 = 1$.

In momentum space, the Hamiltonian for 1D nonreciprocal Su–Schrieffer–Heeger (SSH) model under periodic boundary condition (PBC) can be transformed to

$$\begin{aligned}\hat{H} \to \hat{H}_{\rm PBC}(k) = &\sum_k c_k^\dagger \sigma_x (t_1 + t_2 \cos k) c_k \\ &+ \sum_k c_k^\dagger \sigma_y (t_2 \sin k + i\gamma) c_k \\ &+ \varepsilon \sum_k c_k^\dagger \sigma_z c_k, \end{aligned} \tag{2}$$

where $c_k^\dagger = (c_{k,\rm A}^\dagger, c_{k,\rm B}^\dagger)$; σ_i's are the Pauli matrices acting on the A or B sublattice subspace. For the case of $\varepsilon = 0$, the Hamiltonian $\hat{H}_{\rm PBC}(k)$ has the chiral symmetry, i.e., $\sigma_z \hat{H}_{\rm PBC}(k) \sigma_z = -\hat{H}_{\rm PBC}(k)$. For the case of $\varepsilon \neq 0$, the chiral symmetry is broken.

It was known that due to the NH skin effect, the bulk spectrum of the system becomes that of an NH Hamiltonian $\hat{H}_{\rm OBC}$ under the open boundary condition (OBC). It was pointed out that the physical properties for the 1D nonreciprocal SSH model under the OBC are characterized by $\hat{H}_{\rm OBC}(k)$ rather than $\hat{H}_{\rm PBC}(k)$. As a result, under an NH similarity transformation $\hat{\mathcal{S}}_{\rm NHP}$ the effective bulk Hamiltonian under the OBC turns to[23,24]

$$\begin{aligned}\hat{H} \to \hat{H}_{\rm OBC}(k) = &\sum_k \tilde{c}_k^\dagger [(\bar{t}_1 + \bar{t}_2 \cos k) \sigma_x] \tilde{c}_k \\ &+ \sum_k \tilde{c}_k^\dagger [(\bar{t}_2 \sin k) \sigma_y] \tilde{c}_k \\ &+ \varepsilon \sum_k \tilde{c}_k^\dagger \sigma_z \tilde{c}_k, \end{aligned} \tag{3}$$

where the effective hopping parameters become $\bar{t}_1 = \sqrt{(t_1 - \gamma)(t_1 + \gamma)}$ and $\bar{t}_2 = t_2$. Here, the NH similar-transformation $\hat{\mathcal{S}}_{\rm NHP}$ is really an imaginary gauge transformation, i.e., $c_k^\dagger \to \tilde{c}_k^\dagger = c_{k - iq_0}^\dagger = \hat{\mathcal{S}}_{\rm NHP} c_k^\dagger$ or $c_n^\dagger \to \tilde{c}_n^\dagger = e^{-q_0(n-1)} c_n^\dagger = \hat{\mathcal{S}}_{\rm NHP} c_n^\dagger$ with $e^{q_0} = \sqrt{\frac{t_1 - \gamma}{t_1 + \gamma}}$.

To characterize the topological properties of the NH topological system, the non-Bloch winding number w is introduced.[23] First, we obtain the non-Bloch Hamiltonian from $\hat{H}_{\rm PBC}(k)$ with $\varepsilon = 0$ by the replacement $e^{ik} \to \beta, e^{-ik} \to \beta^{-1}$, i.e., $\hat{H}_{\rm OBC}(\beta) = (t_1 + \gamma + \beta^{-1} t_2)\sigma_+ + (t_1 - \gamma + \beta t_2)\sigma_-$, where $|\beta| = e^{q_0}$ due to $k \mapsto k - iq_0$ in this case. The right/left eigenvectors can be defined $\hat{H}_{\rm OBC}(\beta)$ as $\hat{H}_{\rm OBC}(\beta)|\Psi_{\rm R}\rangle = E(\beta)|\Psi_{\rm R}\rangle, \hat{H}_{\rm OBC}^\dagger(\beta)|\Psi_{\rm L}\rangle = E^*(\beta)|\Psi_{\rm L}\rangle$. Due to the chiral symmetry, we have $|\tilde{\Psi}_{\rm R}\rangle = \sigma_z|\Psi_{\rm R}\rangle$ and $|\tilde{\Psi}_{\rm L}\rangle = \sigma_z|\Psi_{\rm L}\rangle$. Then the non-Bloch winding number based on the generalized Brillouin zone C_β (the trajectory of β) is introduced as $w = \frac{i}{2\pi} \int_{C_\beta} q^{-1} dq$, where q is an off-diagonal member of Q matrix $Q(1,2) = q, Q(2,1) = q^{-1}$, and $Q(\beta) = |\tilde{\Psi}_{\rm R}\rangle\langle\tilde{\Psi}_{\rm L}| - |\Psi_{\rm R}\rangle\langle\Psi_{\rm L}|$. In the region of $|\bar{t}_1| < |\bar{t}_2|$, $w = 1$, the system is a topological insulator. In the region of $|\bar{t}_1| > |\bar{t}_2|$, $w = 0$, the system is a normal insulator. Quantum phase transition occurs at $|\bar{t}_1| = |\bar{t}_2|$, at which the energy gap is closed. In a topological phase, there exist two edge states.

State-Dependent Topological Invariants. Because the non-Bloch topological invariant w cannot predict the existence of the defective edge state, we introduce the state-dependent topological invariants to study the exact formulation of the bulk-boundary correspondence.

Firstly, we decompose $\hat{H}_{\rm PBC}$ into three terms, i.e., $\hat{H}_{\rm PBC} = \hat{H}_{\rm for} + \hat{H}_{\rm back} + \hat{H}_{\rm on}$, where $\hat{H}_{\rm for} = \sum_k c_k^\dagger (h_{\rm for}\sigma^-) c_k$ is the forward hopping term, $\hat{H}_{\rm back} = \sum_k c_k^\dagger (h_{\rm back}\sigma^+) c_k$ is the backward hopping term from, and $\hat{H}_{\rm on}$ is the on-site term, $\hat{H}_{\rm on} = \sum_k c_k^\dagger (\varepsilon\sigma_z) c_k$. Here, we have $h_{\rm for} = (t_1 - \gamma + t_2 e^{ik})$ and $h_{\rm back} = (t_1 + \gamma + t_2 e^{-ik})$. Because ε is considered to be a perturbation, we have $\varepsilon \ll t_2$.

The Hamiltonian $\hat{H}_{\rm PBC}$ possesses a generalized inversion symmetry, i.e.,

$$\hat{\mathcal{I}} \hat{H}_{\rm PBC}(k) \hat{\mathcal{I}}^{-1} = \hat{H}_{\rm PBC}(k)(-k), \tag{4}$$

$$\hat{\mathcal{I}} \hat{H}_{\rm for}(k) \hat{\mathcal{I}}^{-1} = \hat{H}_{\rm for}(-k), \tag{5}$$

$$\hat{\mathcal{I}} \hat{H}_{\rm back}(k) \hat{\mathcal{I}}^{-1} = \hat{H}_{\rm back}(-k), \tag{6}$$

where the inversion operator $\hat{\mathcal{I}}$ is just the time-reversal operator $\mathcal{T}$. This equation implies

$$\mathrm{Re}\, E(k) = \mathrm{Re}\, E(-k), \quad \mathrm{Im}\, E(k) = -\mathrm{Im}\, E(-k). \tag{7}$$

To characterize the nonreciprocal SSH model $\hat{H}_{\rm PBC}$ with the generalized inversion symmetry, we introduce two new topological invariants, i.e., total Z_2 topological invariants $\upsilon_{\rm for} = \upsilon_{{\rm for},k=0}\upsilon_{{\rm for},k=\pi}$ and $\upsilon_{\rm back} = \upsilon_{{\rm back},k=0}\upsilon_{{\rm back},k=\pi}$.

Now, the Bloch Hamiltonian is divided into three parts:

$$\begin{aligned}\hat{H}_{\rm PBC}(k) = &\hat{H}_{\rm for}(k \neq 0/\pi) + \hat{H}_{\rm back}(k \neq 0/\pi) \\ &+ \hat{H}_{\rm for}(k = 0) + \hat{H}_{\rm for}(k = \pi) \\ &+ \hat{H}_{\rm back}(k = 0) + \hat{H}_{\rm back}(k = \pi) + \hat{H}_{\rm on}, \end{aligned} \tag{8}$$

where $k = 0$ and $k = \pi$ are the high symmetry points in momentum space. For $k = 0$, we have

$$\begin{aligned} h_{\rm for}(k = 0) &= t_1 + t_2 - \gamma, \\ h_{\rm back}(k = 0) &= t_1 + t_2 + \gamma; \end{aligned} \tag{9}$$

for $k = \pi$, we have

$$\begin{aligned} h_{\rm for}(k = \pi) &= t_1 - t_2 - \gamma, \\ h_{\rm back}(k = \pi) &= t_1 - t_2 + \gamma. \end{aligned} \tag{10}$$

Thus, to describe $\hat{H}_{\rm PBC}(k)$, we define two Z_2 topological invariants as follows:

$$v_{{\rm for},k=0} = \frac{h_{\rm for}(k=0)}{|h_{\rm for}(k=0)|} = \frac{t_1+t_2-\gamma}{|t_1+t_2-\gamma|}, \quad (11)$$

$$v_{{\rm for},k=\pi} = \frac{h_{\rm for}(k=\pi)}{|h_{\rm for}(k=\pi)|} = \frac{t_1-t_2-\gamma}{|t_1-t_2-\gamma|}, \quad (12)$$

$$v_{{\rm back},k=0} = \frac{h_{\rm back}(k=0)}{|h_{\rm back}(k=0)|} = \frac{t_1+t_2+\gamma}{|t_1+t_2+\gamma|}, \quad (13)$$

$$v_{{\rm back},k=\pi} = \frac{h_{\rm back}(k=\pi)}{|h_{\rm back}(k=\pi)|} = \frac{t_1-t_2+\gamma}{|t_1-t_2+\gamma|}. \quad (14)$$

The two Z_2 topological invariants are defined as

$$v_{\rm for} = v_{{\rm for},{\rm k}=0} v_{{\rm for},k=\pi} = \begin{cases} +1, & \text{trivial phase}, \\ -1, & \text{topological phase}, \end{cases} \quad (15)$$

$$v_{\rm back} = v_{{\rm back},k=0} v_{{\rm back},k=\pi} = \begin{cases} +1, & \text{trivial phase}, \\ -1, & \text{topological phase}. \end{cases} \quad (16)$$

Here $v_{\rm for}$ and $v_{\rm back}$ become two topological invariants to characterize the universal properties of different topological phases for the nonreciprocal SSH model $\hat{H}_{\rm PBC}$ with the generalized inversion symmetry.

Finally, we define the state-dependent topological invariants $\{\bar{v}_{\rm L}, \bar{v}_{\rm R}\}$, where $\bar{v}_{\rm L}$ and $\bar{v}_{\rm R}$ are the topological invariants for the edge states on left and right, respectively. Let us give the detailed definition for $\bar{v}_{\rm L}$ and $\bar{v}_{\rm R}$ as follows:

$$\bar{v}_{\rm L} = w \cdot v_{\rm for}, \quad \bar{v}_{\rm R} = w \cdot v_{\rm back}, \quad (17)$$

where $v_{\rm for}$ and $v_{\rm back}$ are the Bloch Z_2 topological invariants defined from the Hamiltonian under the periodic boundary condition $\hat{H}_{\rm PBC}$, and the non-Bloch winding number w comes from the Hamiltonian under the OBC $\hat{H}_{\rm OBC}$.

In this study, we show that the state-dependent topological invariants $\{\bar{v}_{\rm L}, \bar{v}_{\rm R}\}$ become the complete description of BBC for 1D non-Hermitian topological systems: *Under self-normalization basis, when* $\bar{v}_{\rm L} = 1 (\bar{v}_{\rm L} = -1)$, *the edge state at left end exists (does not exist) and when* $\bar{v}_{\rm R} = 1$ $(\bar{v}_{\rm R} = -1)$, *the edge state at right end exists (does not exist).* In particular, the state-dependent topological invariants $\{\bar{v}_{\rm L}, \bar{v}_{\rm R}\}$ are universal for 1D non-Hermitian topological insulators with the generalized inversion symmetry including the 1D nonreciprocal SSH model with next-nearest neighbor hopping terms.

For the 1D non-Hermitian SSH model, we have two phase diagrams: Fig. 1(a) gives the phase diagram for the edge state characterized by $\bar{v}_{\rm R}$; Fig. 1(b) presents the phase diagram for the edge state characterized by $\bar{v}_{\rm L}$. In the topological phase with $w = 1$ there exist three different phases: the phase with $\bar{v}_{\rm L} = 1$ and $\bar{v}_{\rm R} = 1$, the phase with $\bar{v}_{\rm L} = 1$ and $\bar{v}_{\rm R} = -1$, and the phase with $\bar{v}_{\rm L} = -1$ and $\bar{v}_{\rm R} = 1$. As a result, there exist two kinds of topological phase transitions: one is characterized by the sharp changing of non-Bloch topological invariant w that comes from the gap-closing for $\hat{H}_{\rm OBC}$ at $|\bar{t}_1| = |\bar{t}_2|$, for example, from a trivial phase with $\bar{v}_{\rm L} = \bar{v}_{\rm R} = -1$ (or $w = 0$) to the topological phase with $\bar{v}_{\rm L} \neq -1$ or $\bar{v}_{\rm R} \neq -1$ (or $w = 1$); the other is *state-dependent topological phase transitions* that are characterized by the sharp changing of Bloch topological invariants $v_{\rm for}$ and $v_{\rm back}$ that come from gap-closing for $\hat{H}_{\rm PBC}$ at $t_1 \pm \gamma = \pm t_2$, for example, from a topological phase with the two edge states ($\bar{v}_{\rm L} \cdot \bar{v}_{\rm R} = 1$, and $w = 1$) to another with one edge state ($\bar{v}_{\rm L} \cdot \bar{v}_{\rm R} = -1$, and $w = 1$).

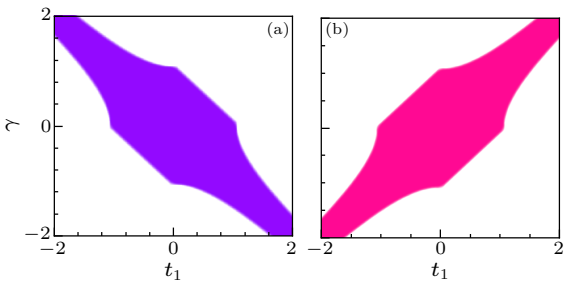

Fig. 1. (a) Global phase diagram for the right edge state. There are two phases with $\bar{v}_{\rm R} = -1$ (the white region) and $\bar{v}_{\rm R} = 1$ (the purple region). (b) Global phase diagram for the left edge state. There are two phases with $\bar{v}_{\rm L} = -1$ (the white region) and $\bar{v}_{\rm L} = 1$ (the pink region).

Effective Hamiltonian for Edge States. In the topological phase with $w = 1$, there exist two edge states for left side and right side under the biorthogonal set, $|b^1\rangle$ and $|b^2\rangle$, respectively. To characterize the physics for edge states in a finite non-Hermitian topological system, we introduce an effective edge Hamiltonian

$$\hat{\mathcal{H}}_{\rm edge} = \begin{pmatrix} h_{11} & h_{12} \\ h_{21} & h_{22} \end{pmatrix}, \quad (18)$$

where $h_{IJ} = \langle b^I|\hat{H}|b^J\rangle$, $I, J = 1, 2$.

Firstly, we consider the Hermitian case with $\gamma = 0$. Now, the wave functions of edge states are given by[15,40] $|b^1\rangle = \frac{1}{\mathcal{N}}\sum_{n=1}^{N}(-\frac{t_1}{t_2})^{n-1}|n\rangle \otimes (1,0)^{\rm T}$, $|b^2\rangle = \frac{1}{\mathcal{N}}\sum_{n=0}^{N-1}(-\frac{t_1}{t_2})^{n}|N-n\rangle \otimes (0,1)^{\rm T}$ with $\mathcal{N} = \sqrt{[1-(\frac{t_1}{t_2})^{2N}]/[1-(\frac{t_1}{t_2})^2]}$ is normalization factor. Here $(1,0)^{\rm T}$ and $(0,1)^{\rm T}$ denote the state vectors of two-sublattices. The orthogonal condition for the two edge states is $\langle b^2|b^1\rangle = 0$. The effective edge Hamiltonian is obtained to be $\hat{\mathcal{H}}_{\rm eff} = \Delta_0\tau^x + \varepsilon\tau^z$ where $\Delta_0 = \frac{(t_2^2-t_1^2)}{t_2}(\frac{t_1}{t_2})^N$. As a result, the energy levels of the two edge states are $E = \pm|E| = \pm\sqrt{\Delta_0^2+\varepsilon^2}$, and the eigenstates $|\psi_+\rangle$ and $|\psi_-\rangle$ read

$$|\psi_+\rangle = \frac{1}{\mathcal{N}_+} \times [(\varepsilon + |E|)|b^1\rangle + \Delta_0|b^2\rangle],$$

$$|\psi_-\rangle = \frac{1}{\mathcal{N}_-} \times [(\varepsilon - |E|)|b^1\rangle + \Delta_0|b^2\rangle], \quad (19)$$

where the normalization factors are

$$\mathcal{N}_+ = \sqrt{(\varepsilon + |E|)^2(\langle b^1|b^1\rangle) + \Delta_0^2(\langle b^2|b^2\rangle)},$$
$$\mathcal{N}_- = \sqrt{(\varepsilon - |E|)^2(\langle b^1|b^1\rangle) + \Delta_0^2(\langle b^2|b^2\rangle)}. \quad (20)$$

In the thermodynamic limit $N \to \infty$, $\Delta_0 \to 0$, we have $E \to \pm\varepsilon$ and $|\psi_+\rangle \to |b^1\rangle$, $|\psi_-\rangle \to |b^2\rangle$.

Next, we consider the NH case. Now, performing the NH similar-transformation $\hat{\mathcal{S}}_{\rm NHP}|n\rangle \to |\bar{n}\rangle = e^{-q_0(n-1)}|n\rangle$ (n denotes the cell number) and replacing t_1 by $\bar{t}_1$ and t_2 by $\bar{t}_2$, we can obtain the wave functions of edge states by

$$|b^1\rangle = \frac{1}{\bar{\mathcal{N}}} \sum_{n=1}^{N} \Big(-\frac{\bar{t}_1}{\bar{t}_2}\Big)^{n-1} e^{q_0(n-1)}|n\rangle \otimes \begin{pmatrix}1\\0\end{pmatrix}$$
$$|b^2\rangle = \frac{1}{\bar{\mathcal{N}}} \sum_{n=0}^{N-1} \Big(-\frac{\bar{t}_1}{\bar{t}_2}\Big)^{n} e^{-q_0 n}|N-n\rangle \otimes \begin{pmatrix}0\\1\end{pmatrix},$$

where $\bar{\mathcal{N}} = \sqrt{[1-(\frac{\bar{t}_1}{\bar{t}_2})^{2N}]/[1-(\frac{\bar{t}_1}{\bar{t}_2})^2]}$ is the normalization factor.

By replacing t_1 by $\bar{t}_1$ and t_2 by $\bar{t}_2$, the effective edge Hamiltonian is obtained as $\bar{\mathcal{H}}_{\rm edge} = \bar{\Delta}\tau^x + \varepsilon\tau^z$, where $\bar{\Delta} = \frac{(\bar{t}_2^2-\bar{t}_1^2)}{\bar{t}_2}(\frac{\bar{t}_1}{\bar{t}_2})^N$. However, to derive the true effective edge Hamiltonian $\breve{\mathcal{H}}_{\rm eff}$, we must perform an additional non-Hermitian similarity transformation $U_{\rm edge}$. With considering the extra non-Hermitian similarity transformation $U_{\rm edge} = \begin{pmatrix}1 & 0\\ 0 & e^{-q_0 N}\end{pmatrix}$, the effective spin model $\bar{\mathcal{H}}_{\rm edge}$ turns into

$$\breve{\mathcal{H}}_{\rm eff} = (U_{\rm edge})^{-1}\bar{\mathcal{H}}_{\rm edge}(U_{\rm edge}) = \begin{pmatrix}\varepsilon & \Delta^+\\ \Delta^- & -\varepsilon\end{pmatrix},$$

where $\Delta^+ = \bar{\Delta}e^{-Nq_0} = \frac{(t_1^2-t_2^2-\gamma^2)}{t_2}(-\frac{t_1^2-\gamma^2}{t_2^2}e^{-2q_0})^{N/2}$ and $\Delta^- = \bar{\Delta}e^{Nq_0} = \frac{(t_1^2-t_2^2-\gamma^2)}{t_2}(-\frac{t_1^2-\gamma^2}{t_2^2}e^{2q_0})^{N/2}$. Under $U_{\rm edge}$, the energy levels do not change, $\bar{E}_\pm = \pm|\bar{E}| = \pm\sqrt{\varepsilon^2+\bar{\Delta}^2}$.

According to the effective edge Hamiltonian $\breve{\mathcal{H}}_{\rm eff}$, the eigenstates of the effective edge Hamiltonian are

$$|\bar{\psi}_+^{\rm R}\rangle = \frac{1}{\bar{\mathcal{N}}_+} \times [(\varepsilon + |\bar{E}|)e^{-q_0 N}|b^1\rangle + \bar{\Delta}|b^2\rangle],$$
$$|\bar{\psi}_-^{\rm R}\rangle = \frac{1}{\bar{\mathcal{N}}_-} \times [(\varepsilon - |\bar{E}|)e^{-q_0 N}|b^1\rangle + \bar{\Delta}|b^2\rangle], \quad (21)$$

where $\bar{\mathcal{N}}_+$ and $\bar{\mathcal{N}}_-$ are the normalized coefficients of $|\bar{\psi}_+^{\rm R}\rangle$ and $|\bar{\psi}_-^{\rm R}\rangle$, respectively. According to $|\langle\bar{\psi}_+^{\rm R}|\bar{\psi}_+^{\rm R}\rangle| = |\langle\bar{\psi}_-^{\rm R}|\bar{\psi}_-^{\rm R}\rangle| = 1$, we have

$$\bar{\mathcal{N}}_+ = \sqrt{(\varepsilon + |\bar{E}|)^2 e^{-2q_0 N}(\langle b^1|b^1\rangle) + \bar{\Delta}^2(\langle b^2|b^2\rangle)},$$
$$\bar{\mathcal{N}}_- = \sqrt{(\varepsilon - |\bar{E}|)^2 e^{-2q_0 N}(\langle b^1|b^1\rangle) + \bar{\Delta}^2(\langle b^2|b^2\rangle)}. \quad (22)$$

State-Dependent Topological Phase Transitions. From the above discussion, in the topological phase, the effective edge Hamiltonian for the two edge states is obtained as $\breve{\mathcal{H}}_{\rm eff} = \bar{\Delta}^+\tau^+ + \bar{\Delta}^-\tau^- + \varepsilon\tau^z$. There exist three phases in thermodynamic limit: (1) phase with $|\bar{\Delta}^+| \to \infty$, $|\bar{\Delta}^-| \to 0$, of which the state-dependent topological invariables are $\bar{v}_{\rm L} = 1$ and $\bar{v}_{\rm R} = 0$; (2) phase with $|\bar{\Delta}^+| \to 0$, $|\bar{\Delta}^-| \to \infty$, of which the state-dependent topological invariables are $\bar{v}_{\rm L} = 0$ and $\bar{v}_{\rm R} = 1$; (3) phase with $|\bar{\Delta}^+| \to 0$, $|\bar{\Delta}^-| \to 0$, of which the state-dependent topological invariables are $\bar{v}_{\rm L} = 1$ and $\bar{v}_{\rm R} = 1$.

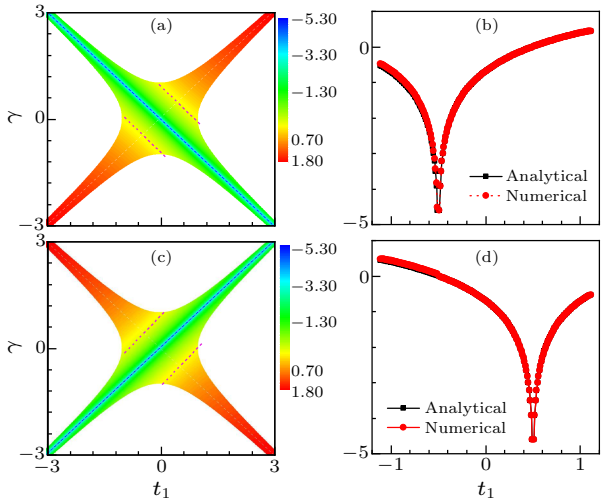

Fig. 2. The numerical results of $\frac{\ln\Delta^+}{N}$ (a) and $\frac{\ln\Delta^-}{N}$ (c) with $N = 50$ and $\varepsilon = 0.01$. The numerical results (red dotted line) and the analytical results (black solid line) of $\frac{\ln\Delta^+}{N}$ (b) and $\frac{\ln\Delta^-}{N}$ (d) with $N = 100$, $\gamma = 0.5$, and $\varepsilon = 0.01$.

As $|\bar{\Delta}^\pm| = \bar{\Delta}e^{\mp Nq_0} = \frac{(t_1^2-t_2^2-\gamma^2)}{t_2}(-\frac{t_1^2-\gamma^2}{t_2^2}e^{\mp 2q_0})^{N/2}$, the state-dependent topological phase transitions occur when $(-\frac{t_1^2-\gamma^2}{t_2^2}e^{\mp 2q_0}) = 1$ in the thermodynamic limit. With setting $t_2 = 1$, we obtain that the state-dependent topological phase transitions occur at $t_1 \pm \gamma = \pm 1$. Figure 2 shows the numerical results for $\frac{\ln\Delta^\pm}{N}$ in which $\frac{\ln\Delta^\pm}{N} = 0$ denotes the state-dependent topological phase transitions. It is obvious that due to $\bar{\Delta} \to 0$, at $\frac{\ln\Delta^\pm}{N} = 0$ the energy levels for the ground states are always $E = \pm\sqrt{\bar{\Delta}^2+\varepsilon^2} \sim \pm\varepsilon$ and show nothing anomalous.

To verify the state-dependent topological phase transitions and show the defectiveness of the edge states, we define the state similarity $|\langle\bar{\psi}_+^{\rm R}|\bar{\psi}_-^{\rm R}\rangle|$, where $|\bar{\psi}_+^{\rm R}\rangle$ and $|\bar{\psi}_-^{\rm R}\rangle$ are the eigenstates for the two edge states under the self-normalization bases, i.e., $|\langle\bar{\psi}_+^{\rm R}|\bar{\psi}_+^{\rm R}\rangle| = |\langle\bar{\psi}_-^{\rm R}|\bar{\psi}_-^{\rm R}\rangle| = 1$. For a defective edge state, if $|\langle\bar{\psi}_+^{\rm R}|\bar{\psi}_-^{\rm R}\rangle|$ is 0, there will be two edge states. If $|\langle\bar{\psi}_+^{\rm R}|\bar{\psi}_-^{\rm R}\rangle| = 1$, there will be one edge state. The sudden changing of state similarity $|\langle\bar{\psi}_+^{\rm R}|\bar{\psi}_-^{\rm R}\rangle|$ indicates the state-dependent topological phase transitions.

Let us show the detailed results for $|\langle\bar{\psi}_+^{\rm R}|\bar{\psi}_-^{\rm R}\rangle|$. The state similarity of the two edge states to be $|\langle\psi_+^{\rm R}|\psi_-^{\rm R}\rangle|$ is obtained as

$$\begin{aligned}&|\langle\bar{\psi}_+^{\rm R}|\bar{\psi}_-^{\rm R}\rangle|\\=&\left[(\varepsilon-|E|)^2e^{-2q_0N}(\langle b^1|b^1\rangle)+\bar{\Delta}^2(\langle b^2|b^2\rangle)\right]^{-1/2}\\&\left[(\varepsilon+|E|)^2e^{-2q_0N}(\langle b^1|b^1\rangle)+\bar{\Delta}^2(\langle b^2|b^2\rangle)\right]^{-1/2}\\&\cdot[(\varepsilon^2-|E|^2)e^{-2q_0N}\langle b^1|b^1\rangle+\bar{\Delta}^2\langle b^2|b^2\rangle],\end{aligned}$$

where

$$\langle b^1|b^1\rangle=\frac{\left[1-(\frac{\bar{t}_1}{\bar{t}_2})^2\right]}{\left[1-(\frac{\bar{t}_1}{\bar{t}_2})^{2N}\right]}\frac{\left[1-(\frac{t_1-\gamma}{\bar{t}_2})^{2N}\right]}{\left[1-(\frac{t_1-\gamma}{\bar{t}_2})^2\right]},$$

$$\langle b^2|b^2\rangle=\frac{\left[1-(\frac{\bar{t}_1}{\bar{t}_2})^2\right]}{\left[1-(\frac{\bar{t}_1}{\bar{t}_2})^{2N}\right]}\frac{\left[1-(\frac{t_1+\gamma}{\bar{t}_2})^{2N}\right]}{\left[1-(\frac{t_1+\gamma}{\bar{t}_2})^2\right]}.$$

The numerical and analytic results for state similarity $|\langle\bar{\psi}_+^{\rm R}|\bar{\psi}_-^{\rm R}\rangle|$ in the case of $N=100$, $\gamma=0.7$, $\varepsilon=0.1$ are given in Fig. 3. The solid lines come from the theoretical prediction and the dots come from the numerical calculations.

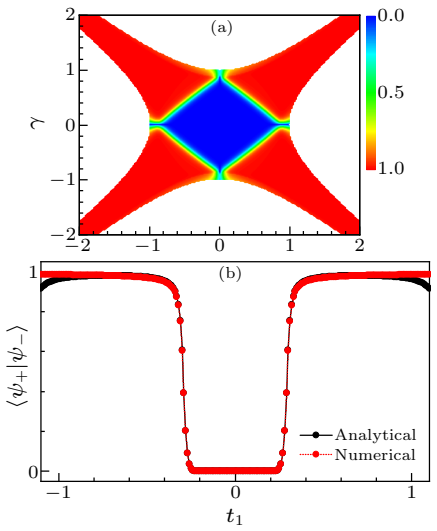

Fig. 3. (a) The state similarity $|\langle\bar{\psi}_+^{\rm R}|\bar{\psi}_-^{\rm R}\rangle|$, i.e., a parameter that characterizes number anomaly of the edge states for the case of $N=20$ and $\varepsilon=0.01$. (b) The state similarity $|\langle\bar{\psi}_+^{\rm R}|\bar{\psi}_-^{\rm R}\rangle|$ for the case of $\gamma=0.3$, $N=100$ and $\varepsilon=0.01$.

In addition, fidelity susceptibilities of edge states $|\bar{\psi}_\pm^{\rm R}\rangle$ can also be used to characterize the state-dependent topological transitions. The fidelities $F_\pm(\gamma,\delta)$ of edge states in terms of γ can be defined as $F_\pm(\gamma,\delta)=|\langle\psi_\pm^{\rm R}(\gamma)|\psi_\pm^{\rm R}(\gamma+\delta)\rangle|$. The fidelity susceptibility of edge states in terms of γ can be defined as $\chi_\pm(\gamma,\delta)=\lim_{(\delta\to0)}\frac{-2\ln F_\pm}{\delta^2}$. Figure 4 shows the fidelity susceptibilities for the wave functions of edge state $|\bar{\psi}_+^{\rm R}\rangle$ or $|\bar{\psi}_-^{\rm R}\rangle$ that indicate the state-dependent topological transitions. We point out that the numerical and analytic results are consistent with each other.

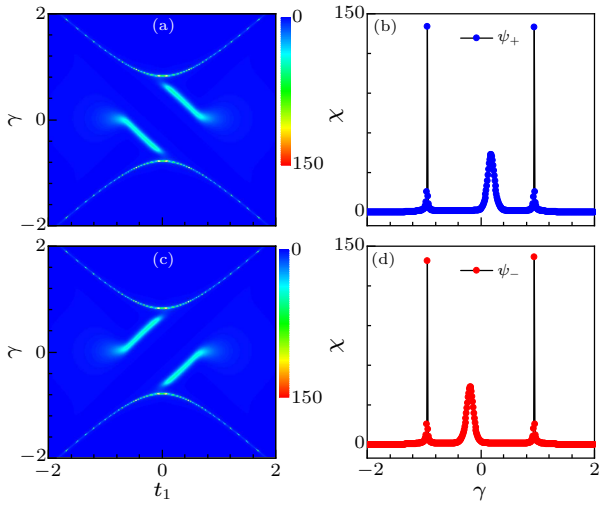

Fig. 4. (a) The fidelity susceptibility for the wave functions of $\bar{\psi}_+^{\rm R}$ in the case of $N=10$ and $\varepsilon=0.01$ via γ and t_1. (b) The fidelity susceptibility for the wave functions of $\bar{\psi}_+^{\rm R}$ in the case of $\gamma=0.3$, $N=10$ and $\varepsilon=0.01$. (c) The fidelity susceptibility for the wave functions of $\bar{\psi}_-^{\rm R}$ in the case of $N=10$ and $\varepsilon=0.01$ via γ and t_1. (d) The fidelity susceptibility for the wave functions of $\bar{\psi}_-^{\rm R}$ in the case of $\gamma=0.3$, $N=10$ and $\varepsilon=0.01$.

In summary, we have developed the theory of state-dependent topological invariants for NH topological insulators with a generalized inversion symmetry. The key point of our theory is that each edge state is characterized by its state-dependent topological invariant $\bar{v}_{\rm L}$ or $\bar{v}_{\rm R}$ rather than a global (state-independent) non-Bloch topological invariant w. With the help of effective edge Hamiltonian $\breve{\mathcal{H}}_{\rm eff}$, we derive the state-dependent phase diagrams and show state-dependent topological transitions. In future, the theory of state-dependent topological invariants can be applied to other types of topological systems with the generalized inversion symmetry, including topological superconductors, higher order topological states, even the topological semi-metals.

References

[1] Hasan M Z and Kane C L 2010 *Rev. Mod. Phys.* **82** 3045
[2] Qi X L and Zhang S C 2011 *Rev. Mod. Phys.* **83** 1057
[3] Thouless D J, Kohmoto M, Nightingale M P and den Nijs M 1982 *Phys. Rev. Lett.* **49** 405
[4] Qi X L, Wu Y S and Zhang S C 2006 *Phys. Rev. B* **74** 085308
[5] Haldane F D M 1988 *Phys. Rev. Lett.* **61** 2015
[6] Kane C L and Mele E J 2005 *Phys. Rev. Lett.* **95** 226801
Kane C L and Mele E J 2005 *Phys. Rev. Lett.* **95** 146802
[7] Alicea J 2012 *Rep. Prog. Phys.* **75** 076501
[8] Chiu C K, Teo J C Y, Schnyder A P and Ryu S 2016 *Rev. Mod. Phys.* **88** 035005
[9] Bansil A, Lin H and Das T 2016 *Rev. Mod. Phys.* **88** 021004
[10] Rudner M S and Levitov L S 2009 *Phys. Rev. Lett.* **102** 065703
[11] Esaki K, Sato M, Hasebe K and Kohmoto M 2011 *Phys. Rev. B* **84** 205128
[12] Kawabata K, Ashida Y, Katsura H and Ueda M 2018 *Phys.*

Rev. B **98** 085116
[13] Liang S D and Huang G Y 2013 *Phys. Rev. A* **87** 012118
[14] Zhu B, Lü R and Chen S 2014 *Phys. Rev. A* **89** 062102
[15] Lee T E 2016 *Phys. Rev. Lett.* **116** 133903
[16] Xu Y, Wang S T and Duan L M 2017 *Phys. Rev. Lett.* **118** 045701
[17] Leykam D, Bliokh K Y, Huang C, Chong Y D and Nori F 2017 *Phys. Rev. Lett.* **118** 040401
[18] Shen H, Zhen B and Fu L 2018 *Phys. Rev. Lett.* **120** 146402
[19] Xiong Y 2018 *J. Phys. Commun.* **2** 035043
[20] Hu Y C and Hughes T L 2011 *Phys. Rev. B* **84** 153101
[21] Gong Z, Ashida Y, Kawabata K, Takasan K, Higashikawa S and Ueda M 2018 *Phys. Rev. X* **8** 031079
[22] Kunst F K, Edvardsson E, Budich J C and Bergholtz E J 2018 *Phys. Rev. Lett.* **121** 026808
[23] Yao S and Wang Z 2018 *Phys. Rev. Lett.* **121** 086803
[24] Yao S, Song F and Wang Z 2018 *Phys. Rev. Lett.* **121** 136802
[25] Yin C, Jiang H, Li L, Lü R and Chen S 2018 *Phys. Rev. A* **97** 052115
[26] Kawabata K, Shiozaki K and Ueda M 2018 *Phys. Rev. B* **98** 165148
[27] Alvarez V M M, Vargas J E B, Berdakin M and Torres L E F F 2018 *Eur. Phys. J. Spec. Top.* **227** 1295
[28] Alvarez V M M, Vargas J E B and Torres L E F F 2018 *Phys. Rev. B* **97** 121401(R)
[29] Jiang H, Yang C and Chen S 2018 *Phys. Rev. A* **98** 052116
[30] McDonald A, Pereg-Barnea T and Clerk A A 2018 *Phys. Rev. X* **8** 041031
[31] Zirnstein H G, Refael G and Rosenow B 2019 arXiv:1901.11241 [cond-mat.mes-hall]
[32] Jin L and Song Z 2019 *Phys. Rev. B* **99** 081103
Lin S, Jin L and Song Z 2019 *Phys. Rev. B* **99** 165148
Zhang K L, Wu H C, Jin L and Song Z 2019 *Phys. Rev. B* **100** 045141
[33] Lee C H and Thomale R 2019 *Phys. Rev. B* **99** 201103(R)
Lee C H, Li G, Liu Y, Tai T, Thomale R and Zhang X 2018 arXiv:1812.02011 [cond-mat.mes-hall]
[34] Liu T, Zhang Y R, Ai Q, Gong Z, Kawabata K, Ueda M and Nori F 2019 *Phys. Rev. Lett.* **122** 076801
[35] Kawabata K, Shiozaki K, Ueda M and Sato M 2019 *Phys. Rev. X* **9** 041015
[36] Zhou H and Lee J Y 2019 *Phys. Rev. B* **99** 235112
[37] Liu C H, Jiang H and Chen S 2019 *Phys. Rev. B* **99** 125103
[38] Herviou L, Bardarson J H and Regnault N 2019 *Phys. Rev. A* **99** 052118
[39] Yokomizo K and Murakami S 2019 *Phys. Rev. Lett.* **123** 066404
[40] Chen R, Chen C Z, Zhou B and Xu D H 2019 *Phys. Rev. B* **99** 155431
[41] Deng T S and Yi W 2019 *Phys. Rev. B* **100** 035102
[42] Song F, Yao S and Wang Z 2019 *Phys. Rev. Lett.* **123** 170401
[43] Song F, Yao S and Wang Z 2019 *Phys. Rev. Lett.* **123** 246801
[44] Luo X W and Zhang C 2019 *Phys. Rev. Lett.* **123** 073601
[45] Okuma N and Sato M 2019 *Phys. Rev. Lett.* **123** 097701
[46] Bergholtz E J and Budich J C 2019 *Phys. Rev. Res.* **1** 012003(R)
[47] Lee J Y, Ahn J, Zhou H and Vishwanath A 2019 *Phys. Rev. Lett.* **123** 206404
[48] Rui W B, Hirschmann M M and Schnyder A P 2019 *Phys. Rev. B* **100** 245116
[49] Schomerus H 2020 *Phys. Rev. Res.* **2** 013058
[50] Imura K I and Takane Y 2019 *Phys. Rev. B* **100** 165430
[51] Herviou L, Regnault N and Bardarson J H 2019 *SciPost Phys.* **7** 069
[52] Chang P Y, You J S, Wen X and Ryu S 2020 *Phys. Rev. Res.* **2** 033069
[53] Zhang X X and Franz M 2020 *Phys. Rev. Lett.* **124** 046401
[54] Zhang K, Yang Z and Fang C 2019 arXiv:1910.01131 [cond-mat.mes-hall]
Yang Z, Zhang K, Fang C and Hu J 2019 arXiv:1912.05499 [cond-mat.mes-hall]
[55] Okuma N, Kawabata K, Shiozaki K and Sato M 2020 *Phys. Rev. Lett.* **124** 086801
[56] Longhi S 2020 *Phys. Rev. Lett.* **124** 066602
[57] Wang X R, Guo C X and Kou S P 2020 *Phys. Rev. B* **101** 121115(R)
[58] Yoshida T, Mizoguchi T and Hatsugai Y 2020 *Phys. Rev. Res.* **2** 022062
[59] Kawabata K, Okuma N and Sato M 2020 arXiv:2003.07597v1 [cond-mat.mes-hall]
[60] Wang C, Wang X R, Guo C X and Kou S P 2020 *Int. J. Mod. Phys. B* **34** 20501465
[61] Yang M L, Wang H, Guo C X, Wang X R, Sun G Y and Kou S P 2020 arXiv:2006.10278V2 [cond-mat.str-el]
[62] Zhao X M, Guo C X, Yang M L, Wang H, Liu W M and Kou S P 2020 arXiv:2007.03864V1 [cond-mat.mes-hall]
[63] Zeuner J M, Rechtsman M C, Plotnik Y, Lumer Y, Nolte S, Rudner M S, Segev M and Szameit A 2015 *Phys. Rev. Lett.* **115** 040402
[64] Weimann S, Kremer M, Plotnik Y, Lumer Y, Nolte S, Makris K G, Segev M, Rechtsman M C and Szameit A 2017 *Nat. Mater.* **16** 433
[65] Xiao L, Zhan X, Bian Z H, Wang K K, Zhang X, Wang X P, Li J, Mochizuki K, Kim D, Kawakami N, Yi W, Obuse H, Sanders B C and Xue P 2017 *Nat. Phys.* **13** 1117
[66] Zhou H, Peng C, Yoon Y, Hsu C W, Nelson K A, Fu L, Joannopoulos J D, Soljačić M M and Zhen B 2018 *Science* **359** 1009
[67] Bandres M A, Wittek S, Harari G, Parto M, Ren J, Segev M, Christodoulides D N and Khajavikhan M 2018 *Science* **359** 4005
Harari G, Bandres M A, Lumer Y, M, Rechtsman C, Chong Y D, Khajavikhan M, Christodoulides D N and Segev M 2018 *Science* **358** eaar4003
[68] Cerjan A, Huang S, Wang M, Chen K P, Chong Y and Rechtsman M C 2019 *Nat. Photon.* **13** 623
[69] Wang K, Qiu X, Xiao L, Zhan X, Bian Z, Sanders B C, Yi W and Xue P 2019 *Nat. Commun.* **10** 2293
[70] Zhao H, Qiao X, Wu T, Midya B, Longhi S and Feng L 2019 *Science* **365** 1163
[71] Brandenbourger M, Locsin X and Lerner E 2019 *Nat. Commun.* **10** 4608
Ghatak A, Brandenbourger M, van Wezel J and Coulais C 2019 arXiv:1907.11619 [cond-mat.mes-hall]
[72] Xiao L, Deng T, Wang K, Zhu G, Wang Z, Yi W and Xue P 2020 *Nat. Phys.* **16** 761
[73] Helbig T, Hofmann T, Imhof S, Abdelghany M, Kiessling T, Molenkamp L W, Lee C H, Szameit A, Greiter M and Thomale R 2020 *Nat. Phys.* **16** 747